A comparison of the low-frequency vibrational spectra of liquids obtained through infrared and Raman spectroscopies

Gerard Giraud and Klaas Wynne[a)]
Department of Physics, University of Strathclyde, 107 Rottenrow, Glasgow G4 0NG, Scotland, United Kingdom

(Received 19 May 2003; accepted 11 September 2003)

Dynamic solvation of charge-distribution rearrangements is often described using a (harmonic) solvent coordinate. It is not *a priori* clear whether such a solvent coordinate has a real physical meaning. We have studied five polar organic liquids (benzonitrile, benzyl alcohol, *N*,*N*-dimethylformamide, ethylene glycol, and glycerol triacetate) with high-resolution high signal-to-noise ultrafast optical heterodyne-detected Raman-induced optical Kerr effect spectroscopy (OHD-RIKES). The data, converted to the frequency domain, were analyzed entirely with a multimode Brownian-oscillator model. The infrared spectra of the same five liquids were obtained with a combination of terahertz spectroscopy and Fourier-transform infrared spectroscopy. The Brownian-oscillator fits to the OHD-RIKES spectra could be converted successfully to IR spectra by using a simple theoretical model and by keeping all Brownian-oscillator parameters the same except for the amplitudes. This suggests that there is a small set of harmonic oscillators describing ultrafast solvent nuclear dynamics that can be used to understand solvation, IR absorption, and Raman scattering spectra. © *2003 American Institute of Physics.*
[DOI: 10.1063/1.1623747]

I. INTRODUCTION

Condensed-phase chemical reactions are in large part controlled by the static and dynamic influences of the surrounding solvent. Especially in the case of very fast (sub)picosecond reactions, it is the solvent-induced dephasing of intramolecular vibrations and the exchange of energy with the bath that determines the reaction rate more so than the shape of the intramolecular vibrational potentials. For example, in ultrafast condensed-phase electron-transfer,[1–3] it is often found that the reaction rate is strongly correlated with the solvent dynamics. The reason is that fluctuations in the surrounding solvent bring the system in a region where the reaction can take place and once in this region, again the solvent fluctuations largely determine the probability for jumping from one electronic surface to another.[4–7] However, the correlation between solvent dynamics and the rate of chemical reactions is not well understood quantitatively. There are two main reasons for this: First, of all the dynamics of the solvent itself (in the absence of a solute that may undergo a chemical reaction), especially on a short subpicosecond time scale, has been characterized experimentally over the years but is still not understood very well in terms of a microscopic picture. Second, once the pure solvent dynamics has been analyzed, there remains the problem of understanding the coupling between the solvent and the solute.[8]

Over the past decade and more, liquid dynamics has been studied in great detail in a great variety of liquids and liquid mixtures using the optical heterodyne-detected Raman-induced Kerr-effect spectroscopy (OHD-RIKES) technique.[9] As technology has improved (and laser pulses became shorter), attention has shifted from the long-time ($\approx 1-100$ ps) diffusive reorientational dynamics of the liquids[10,11] to the short time (≈ 10 fs to 1 ps) inertial dynamics.[12] Improved technology now also allows the measurement of the OHD-RIKES spectra of dissolved organic molecules[13] and even peptides and proteins[14–16] and inhomogeneous systems such as nanoporous glasses.[17] OHD-RIKES is a time-resolved four-wave mixing experiment but the resultant signal is essentially proportional to (the Fourier-transform of) the depolarized Raman spectrum of the liquid[9] albeit with superior signal-to-noise ratio at low frequencies (<400 cm^{-1}). Broadly speaking, one can discern two components in the low-frequency spectrum: A sharp Lorentzian feature around zero frequency and a broad bell-shaped feature. The Lorentzian line is due to the slow diffusive reorientational response of the solvent molecules[11] and corresponds to an exponential decay on a 1–100 ps time scale in the time-domain. The bell-shaped feature (sometimes there are multiple such features) is due to the inertial response of the liquid, that is, the dynamics that is not strongly overdamped. These inertial motions of the liquid may be librational or translational in character and include the inertially limited rotation of the molecules (gas-phaselike free rotation). Unfortunately, the bell-shaped curve is essentially featureless, which makes a full understanding of the microscopic dynamics that gives rise to it hard to attain.

Recently attempts have been made to use higher-order Raman-like spectroscopies to access hidden information in the solvent Raman bands.[18–20] It was shown theoretically[21–24] that off-resonant six- and eight-wave mixing experiments can in principle be used to access information that

[a)]Electronic mail: klaas.wynne@phys.strath.ac.uk; Phone: +44 (141) 548-3381; URL: http://dutch.phys.strath.ac.uk

is unavailable from the OHD-RIKES type experiments. Several of these experiments have been performed on low-frequency solvent modes, however, their interpretation is hampered by the presence of ''contamination'' from cascaded lower-order processes.[20,25] It appears that a full explanation of these experimental results is not yet available.

The dynamics of the solvent–solute interaction is typically studied using dyes that undergo a large change in permanent dipole moment upon excitation to the first electronically excited state. For example, the time-dependent fluorescence spectrum[11,26] can be measured on an ultrafast time scale (the dynamic Stokes shift). The time-dependent redshift of the spectrum is due to the dynamic solvation of the new permanent dipole moment by the surrounding solvent. Similarly, photon echo experiments[27] on these dyes in solution can be related to the bath dynamics. It was realized that the dynamic Stokes shift and photon echo experiments could be related to the pure solvent dynamics as obtained with an OHD-RIKES experiment.[28] The relation has been tested on just a few solvents notably acetonitrile. This relation between two quite different experiments is based on certain assumptions[29,30] and has caveats that will be discussed below in more detail. The main assumption is that the solvent has a distribution of low-frequency modes (the solvent spectral density) and that these modes give rise to the Raman spectrum, the IR spectrum, and the spectrum of solvation.[31] It ignores the possibility that certain modes might be more effective in Raman scattering while being less effective at solvating. It is essentially this assumption that we would like to test.

The frequency-response functions obtained through OHD-RIKES experiments are typically fitted to three or four functions:[9] A Lorentzian (corresponding to rotational diffusion), an Ohmic function (representing a collisional process[32] or collective translational motions), and a number of Gaussian functions (corresponding to translational or librational motion). This set of functions seems to fit the spectra of all solvents studied with OHD-RIKES so far although there is no proper physical reason why this should be so. For example, the Ohmic function is meant to describe[32] a line shape due to a collision-induced anisotropy of the polarizability whereas in many cases the molecular anisotropic polarizability will dominate the Raman spectrum.[33] The Gaussian line shapes are justified based on a model in which librating molecules find themselves in solvent cavities whose parameters are inhomogeneously (statically) distributed throughout the solvent.[34] However, there is little evidence of inhomogeneous broadening in liquids.[35]

Another method for fitting low-frequency vibrational spectra is based on the Brownian-oscillator model.[29] On short time scales, the interaction potentials between the molecules in the liquid can be Taylor expanded to second order implying harmonic motion on these time scales.[36] The Brownian-oscillator model in effect assumes that the 10^{23} or so harmonic oscillators in a liquid sample may be rearranged as a limited number of characteristic modes with the remainder of the solvent motions responsible for damping through cubic terms in the potential expansion.[37] Here, we will take this model to its extreme by assuming that as little as four homogeneously damped Brownian oscillators may describe solvent motions.

If the assumption that a single distribution of low-frequency Brownian solvent modes gives rise to the Raman, the IR and the solvation spectrum holds true, then the IR spectrum should be identical in structure to the Raman spectrum. The strength of IR absorption and the efficiency of Raman scattering depend on different physical properties of the molecules involved and therefore the relative amplitude of the various Brownian-oscillator components is expected to be different. Unfortunately, obtaining the IR spectrum in the relevant spectral region ($\approx 0-300\ \mathrm{cm}^{-1}$) is experimentally nontrivial, as the lowest accessible frequency for most IR spectrometers is about $400\ \mathrm{cm}^{-1}$. Even spectrometers equipped with bolometric detectors can go no lower than about $25\ \mathrm{cm}^{-1}$ because no light sources powerful enough in this range are available.

Significant developments have taken place in the coherent generation and detection of light pulses in the far-infrared or THz range.[38] The most common technique for generating THz pulses has been the use of Auston photoconductive switches or biased dipolar antennas.[39] In this technique, two biased metal electrodes, laid down on a semiconductor substrate, are irradiated at the gap between the electrodes with a femtosecond near-IR laser pulse. This induces a transient current that radiates an electromagnetic field in the THz frequency-range. THz pulses generated in this manner typically have a spectrum that peaks at $\approx 10\ \mathrm{cm}^{-1}$ and a usable bandwidth up to frequencies as high as $60\ \mathrm{cm}^{-1}$.[40–42] More recently, a technique based on optical rectification and electro-optic sampling has been used to generate and detect THz pulses.[43,44] With this detection technique, the bandwidth can be increased to frequencies as high as $1200\ \mathrm{cm}^{-1}$ (37 THz).[45,46] Generation of THz pulses by optical rectification[43,47] in a nonlinear crystal such as GaAs or ZnTe combined with Pockels-effect detection results in a system with the greatest usable bandwidth. The THz-pulse technique has two significant advantages: The detection is gated with a window on the order of 100 fs thereby effectively eliminating background thermal noise and the detection is coherent (the electric field rather than the intensity is measured), which allows one to extract both the absorption coefficient and the refractive index. The technique has been used by a number of groups to study the FIR absorption in the very low-frequency ($\approx 0-100\ \mathrm{cm}^{-1}$) range of several nonpolar[48–52] and polar liquids.[53–58] In these studies, the experimental spectral range was either not large enough to cover the entire low-frequency solvent absorption band or no attempt was made to compare the FIR spectrum with the Raman spectrum. We will try to remedy this situation by combining THz-spectroscopy with FTIR spectroscopy. The range of our THz spectrometer is $1-85\ \mathrm{cm}^{-1}$. The range of the FTIR spectrometer is $25-600\ \mathrm{cm}^{-1}$ and these data are patched onto the THz data. The resultant IR spectra in the range $1-300\ \mathrm{cm}^{-1}$ have been compared with the equivalent Raman spectra as obtained through OHD-RIKES spectroscopy.

II. THEORY

The aim is to calculate the spectrum of the solvent at low frequencies, that is, at frequencies comparable to k_BT. The dielectric function can be expressed as a function of the commutator of the dipole-moment operator as[52,59,60]

$$\tilde{\varepsilon}(\omega) = -\int_0^\infty dt_1 e^{+i\omega t_1}\chi_{\mu\mu}(t_1), \tag{1}$$

where

$$\chi_{\mu\mu}(t) = N(i\hbar)^{-1}\langle[\hat{\mu}(t),\hat{\mu}(0)]\rangle_{\mathrm{eq}}. \tag{2}$$

Here the angled brackets stand for a trace over the equilibrium density matrix and the square brackets for the commutation operation. Here the caret denotes an operator in Hilbert-space. Propagation of the field through the sample as plane waves in the z-direction can be described by

$$\tilde{E}(z,\omega) = \tilde{E}(z=0,\omega)\exp(i\omega z\tilde{n}(\omega)/c), \tag{3}$$

where the complex refractive index is given by $\tilde{n}(\omega) = \sqrt{\tilde{\varepsilon}(\omega)}$. This may then be related to the (real) refractive index $n(\omega)$ and absorption coefficient $\alpha(\omega)$ using

$$\tilde{n}(\omega) = (n(\omega) + ic\alpha(\omega)/(2\omega)). \tag{4}$$

Using these expressions does not involve the slowly-varying envelope approximation.[61] Only in the limit of $\mathrm{Im}\,\tilde{\varepsilon}\to 0$ can the absorption coefficient be approximated as $\alpha \cong \omega\,\mathrm{Im}\,\tilde{\varepsilon}/(cn)$.

The OHD-RIKES signal and spectrum have been calculated before.[9,29,62,63] In the slowly varying envelope approximation the signal in the time domain is given by

$$S(\tau) = \frac{\omega_2 z}{\varepsilon_0^3 c}\int_0^\infty dt' G(\tau - t')\chi_{\alpha\alpha}(t'), \tag{5}$$

where

$$\chi_{\alpha\alpha}(t) = N(i\hbar)^{-1}\langle[\hat{\alpha}_{22}(t),\hat{\alpha}_{11}(0)]\rangle_{\mathrm{eq}}, \tag{6}$$

and $G(t)$ is the intensity cross-correlation function of the pump and the probe pulse and τ is the temporal delay between these pulses. Typically, the time-dependent OHD-RIKES signal is Fourier-transformed and deconvoluted in order to calculate the frequency-dependent OHD-RIKES response function, i.e.,

$$\tilde{S}_{\mathrm{OKE}}(\omega) \equiv \frac{\tilde{S}(\omega)}{\tilde{G}(\omega)} = \frac{\omega_{\mathrm{laser}} z}{\varepsilon_0^3 c}\int_0^\infty dt\,\chi_{\alpha\alpha}(t)e^{+i\omega t}. \tag{7}$$

The experimental OHD-RIKES data presented here will always be shown in this deconvoluted form.

Thus, both the IR and OHD-RIKES spectra are proportional to the Fourier transform of a response function.[59] In the case of the IR spectrum, it is the response function of the dipole moment (operator) and in the case of Raman scattering, it is that of the polarizability (operator). Both can be put on an equal footing, however, under some reasonable assumptions. The most obvious difference between $\chi_{\mu\mu}$ and $\chi_{\alpha\alpha}$ is that the former is the ensemble average of a second-order tensor and the latter that of a fourth-order tensor in the dipole moment. Here it will be assumed for simplicity that the orientational diffusion component of $\chi_{\mu\mu}$ and $\chi_{\alpha\alpha}$ is relevant on a much longer time scale (picoseconds) than the translational and librational motions (subpicosecond) of interest here, and can be ignored or be dealt with separately.[11] This assumption amounts to making the separation of the itinerant-oscillator model.[64]

The polarizability has a weak dependence on the (intra- or intermolecular) nuclear coordinates and can be expanded around the equilibrium configuration q_0 as

$$\hat{\alpha}(q) = \hat{\alpha}_0 + \sum_i \left(\frac{\partial\alpha}{\partial q_i}\right)_{q=q_0}\hat{q}_i + \cdots, \tag{8}$$

where the sum runs over all the nuclear coordinates. Therefore, the response function for OHD-RIKES can be written as

$$\chi_{\alpha\alpha}(t) = N(i\hbar)^{-1}\sum_i \langle(\alpha_i')^2[\hat{q}_i(t),\hat{q}_i(0)]\rangle_{\mathrm{eq}}, \tag{9}$$

where $\langle\cdots\rangle_{\mathrm{eq}}$ is an ensemble average. Similarly, in the Born–Oppenheimer approximation, the dipole-moment operator can be expanded as

$$\hat{\mu}(q) = \hat{\mu}_0 + \sum_i \left(\frac{\partial\mu}{\partial q_i}\right)_{q=q_0}\hat{q}_i + \cdots, \tag{10}$$

and the response function for IR absorption becomes

$$\chi_{\mu\mu}(t) = N(i\hbar)^{-1}\sum_i \langle(\mu_i')^2[\hat{q}_i(t)\hat{q}_i(0)]\rangle_{\mathrm{eq}}. \tag{11}$$

Therefore, apart from the prefactor $(\alpha_i')^2$ or $(\mu_i')^2$, the two response functions are the same. Hence, the IR and Raman spectra are in principle determined by the same vibrational (librational, translational) solvent modes. In molecules with a center of inversion, symmetry dictates that those intramolecular modes that are IR active are not Raman active and vice versa. However, one does not expect symmetry in a liquid and therefore the same intermolecular modes in principle could be both IR and Raman active. The question we hope to answer here is whether the low-frequency IR and Raman spectra have the same structure, i.e., whether the relative magnitudes of the prefactors in Eq. (9) are essentially the same as those in Eq. (11). If this were the case, the Raman (OHD-RIKES) spectrum could be converted into an IR spectrum[31,64] since the OHD-RIKES spectrum is proportional to the Fourier transform of Eq. (9) and the IR spectrum (at least in the limit of $\mathrm{Im}\,\tilde{\varepsilon}\to 0$) proportional to the Fourier transform of Eq. (11).

In general, it is difficult to predict the strength of IR absorption and Raman scattering, or the magnitude of μ' and α' theoretically. It is instructive, however, to calculate these quantities in a simplified two-dimensional classical model. This simple model ignores collective (translational) motions and assumes that the strength of IR absorption and Raman scattering is largely determined by single-molecule properties.[33,60,65] Intramolecular vibrational motions change molecular bond lengths and can therefore be expected to

change the permanent dipole moment or the polarizability of a molecule. In the absence of hard collisions, intermolecular motions are not expected to change the molecular dipole moment or polarizability within the molecular coordinate frame. Collisions can change the molecular polarizability but this is expected to have a relatively minor effect in polar liquids[33,60] and only in the high-frequency tail of the spectra.[32,66] Therefore, the only way that an intermolecular motion can change the dipole moment or polarizability is by changing the projection onto the laboratory coordinate axes.

Consider a simple two-dimensional model consisting of a rigid body with permanent dipole moment μ in a force field consisting of interactions with neighboring molecules. On short timescales, it may be assumed[36] that these forces can be approximated by a harmonic force as a function of the angle of the molecule, resulting in librational motion. The equilibrium angle for the librator is θ_0 and any external force will displace it perturbatively to θ so that $\theta=\theta_0$ at equilibrium. In an ensemble of librators, there will be a distribution of equilibrium angles. In this model, the dipole moment derivative is

$$\mu' = \mu \begin{pmatrix} -\sin(\theta_0) \\ \cos(\theta_0) \end{pmatrix}. \tag{12}$$

An external polarized electric field will exert a force $\mathbf{F}=-\boldsymbol{\mu}'\cdot\mathbf{E}$ onto each molecule, rotating each slightly, and inducing a macroscopic polarization in the sample. Using a classical Langevin-equation approach,[67] it is straightforward to calculate the macroscopic polarization in response to an external field. With the definition of the susceptibility $\mathbf{P}(\omega)=\hat{\chi}(\omega)\cdot\mathbf{E}(\omega)$ and the dielectric function $\hat{\varepsilon}(\omega)=\hat{1}+\hat{\chi}(\omega)$, and after averaging over a homogeneous distribution of equilibrium orientations, the expression

$$\hat{\varepsilon}(\omega)=\hat{1}+\tfrac{1}{2}\hat{1}N\mu^2 I^{-1}[(\omega-\omega_+)(\omega-\omega_-)]^{-1} \tag{13}$$

can be derived, where N is the number density, I is the moment of inertia, $\omega_\pm=-i\gamma/2\pm\Omega$, γ is the damping rate, $\Omega\equiv(\omega_0^2-\gamma^2/4)^{1/2}$, ω_0 is the librational frequency in the absence of damping, and $\hat{1}$ is the unity matrix. The absorption described by Eq. (13) is known as Poley absorption.[64]

In the two-dimensional harmonic librator model, the derivative of the polarizability matrix with respect to the equilibrium angle is

$$\hat{\alpha}' = \overline{\alpha}' \begin{pmatrix} \sin 2\theta_0 & -\cos 2\theta_0 \\ -\cos 2\theta_0 & \sin 2\theta_0 \end{pmatrix}. \tag{14}$$

A rigid body with a permanent dipole moment is polarizable because it can rotate with respect to the laboratory axes. Therefore, the polarizability derivative has two contributions: A polarizability resulting from the presence of a permanent dipole moment $\hat{\alpha}'_{\text{dipole}}$ and a polarizability intrinsic to the molecule $\hat{\alpha}'_{\text{intrinsic}}$ (the electronic polarizability). Both components have the same orientational dependence [Eq. (14) for two dimensions]. In the case of a symmetric top, the prefactor $\overline{\alpha}'$ in Eq. (14) for $\hat{\alpha}'_{\text{intrinsic}}$ is given by the anisotropic part of the intrinsic polarizability tensor $(\alpha_\parallel-\alpha_\perp)$ with θ_0 corresponding to the angle between the molecular symmetry axis and the laboratory axis.[11] For the polarizability due to the presence of a permanent dipole moment, $\overline{\alpha}'$ in Eq. (14) is given by $\mu^2/I\omega_{\text{laser}}^2$ and θ_0 corresponds to the angle of the permanent dipole moment with respect to the laboratory axis. The OHD-RIKES signal depends on the orientational average of the difference between $\alpha'_{xx}\alpha'_{xx}$ and $\alpha'_{xx}\alpha'_{yy}$.[29] Performing this average after calculating the sample polarization in much the same way as for the dielectric function, it is found

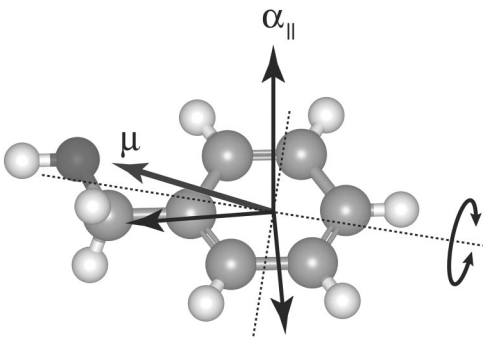

FIG. 1. Schematic illustration of librational motion of benzyl alcohol along three inertial axes. In a molecule without symmetry, the inertial axes are not necessarily parallel to the eigenvectors of the polarizability tensor or to the permanent dipole moment vector.

$$S_{xxxx-xxyy} \propto N(\overline{\alpha}')^2 I^{-1}[(\omega-\omega_+)(\omega-\omega_-)]^{-1}. \tag{15}$$

Comparing Eqs. (13) and (15), it is clear that the IR and OHD-RIKES spectra have a nearly identical functional form. Only in the case of nonpolarizable molecules, when $\overline{\alpha}'=\mu^2/I\omega_{\text{laser}}^2$, can Eqs. (13) and (15) be used to convert a Raman spectrum into an IR spectrum and vice versa. However, in practice the intrinsic electronic anisotropic polarizability is several orders of magnitude larger than the polarizability that results from the presence of a permanent dipole moment.[68] The two-dimensional model could easily be extended to three dimensions, however, the main result is the same in two and three dimensions: The IR absorption strength is determined by the permanent dipole moment of the molecules undergoing librational motion whereas the Raman scattering strength is determined by the magnitude of the anisotropic part of the electronic polarizability tensor. Thus, in principle *there is no simple relationship between Raman and IR spectra*.

The lack of a relationship between Raman and IR spectra certainly holds true for high frequency intramolecular vibrational modes. However, the librational modes studied here are intermediate in frequency ($\sim$10–150 cm^{-1}), have large amplitude, and have a decidedly intermolecular character, and as a result, a relationship could possibly exist. It is unlikely that such a relationship would exist for the very low frequency ($\lesssim$10 cm^{-1}) diffusive modes. Figure 1 shows a schematic diagram of benzyl alcohol. The intrinsic polarizability of the molecule is mostly due to the π electrons and therefore the eigenvectors of the polarizability tensor will be aligned with the phenyl-ring structure. The permanent dipole moment (which gives rise to Poley absorption), however, will be mostly aligned with the OH bond. The inertial axes of an asymmetric molecule will not necessarily be parallel to

either the eigenvectors of the polarizability tensor or the permanent dipole-moment vector. As a result, all three possible librational motions will be both Raman and IR active to some extent.

Librational motion of a molecule in a liquid takes place in a cavity formed by neighboring molecules and this cavity changes rapidly due to the librations of the neighboring molecules and due to diffusion. As a result, it is likely that the three librational modes of any given nonsymmetric molecule will be anharmonically coupled[37] giving rise to energy transfer between the modes. If this energy transfer is rapid compared to the frequency of the modes, it will again make all three librational modes both IR and Raman active. The same argument applies to translational modes, which can be seen as librations of a cage formed by a small number of neighboring molecules.[34]

Thus, it is sensible to perform experiments to determine whether there exists a simple relationship between the low-frequency IR and Raman/OHD-RIKES spectra. This relationship may be expected to be stronger in polar molecules with a large electronic polarizability anisotropy[33] and much weaker in nonpolar molecules with a large interaction-induced component to the spectra. To determine a relationship between IR and Raman spectra, the experimental spectra have to be fitted to functions with each representing a class of motions.

Typically, the experimental spectrum that is obtained from an OHD-RIKES experiment is fitted to a number of theoretical functions.[9] The low-frequency part ($0-10\ \mathrm{cm}^{-1}$, typically associated with diffusive reorientational motion of the liquid) is often fitted with one or two Lorentzian functions. The midfrequency part ($10-100\ \mathrm{cm}^{-1}$, associated with translational and librational motions of the solvent molecules) tends to be fitted to the Ohmic function[32] $r(\omega)=(\omega/\omega_c)\exp(-\omega/\omega_c)$. Higher frequency components ($>100\ \mathrm{cm}^{-1}$) are often fitted to Gaussian functions. However, based on the simple analysis above, it would appear more logical to describe the ultrafast motions in a liquid as the harmonic motions along the various nuclear coordinates q_i. Such a Brownian-oscillator description is akin to the instantaneous normal-mode picture of short-time-scale solvent motions.[33,36,60,66] It is equivalent to assuming that the intermolecular forces can be expanded to second order in the nuclear coordinates at any given instant in time.

In this view of the solvent, N solvent molecules will give rise to $6N$ harmonic oscillators damped through cubic terms in the expansion of the potential.[37] However, many of the $6N$ oscillators will have a similar character, for example, $3N$ oscillators may correspond to what might be described as single-molecule librational motion and the remaining $3N$ oscillators as translational (including cage librations). If fluctuations are fast and of small amplitude (the ''fast modulation limit'') damping is homogeneous, and it is difficult to distinguish the individual oscillators. Therefore, it may be expected that only a small number of ''important'' oscillatory motions characterize the ultrafast motions in a liquid. This picture is different from the conventional Brownian-oscillator model as used to describe various spectroscopies in molecules: A given ''important'' oscillatory motion (e.g., libration of a solvent molecule around a particular axis) may occur about N times in the sample. For each molecule (or group of molecules) undergoing librational motion, the remainder of the liquid [and its $\sim 6(N-1)$ modes] acts as a ''bath'' causing damping. This picture is consistent with a recent instantaneous normal-mode treatment,[37] which showed that the most important source of damping is modes of similar frequency. Thus, the important oscillators can be described by a Langevin model and in the Markovian approximation, the response function can be written as[29,62,63,69]

$$r(t)=N(i\hbar)^{-1}\sum_i \langle[\hat{q}_i(t)\hat{q}_i(0)]\rangle_{\mathrm{eq}}$$

$$=N\theta(t)\sum_i B_i(m_i\Omega_i)^{-1}e^{-\gamma_i t/2}\sin\Omega_i t, \tag{16}$$

where $\theta(t)$ is the Heaviside step function, $\Omega_i\equiv(\omega_i^2-\gamma_i^2/4)^{1/2}$, m_i is the effective mass of the Brownian oscillator, γ_i is its damping rate, and ω_i is its frequency in the absence of damping. The sum in Eq. (16) runs over the small subset of important oscillatory motions. The response function for a single oscillator can be written in the frequency domain as

$$\tilde{r}(\omega)=4Nm_i^{-1}[(\gamma_i-2i\omega)^2+4\Omega_i^2]^{-1}. \tag{17}$$

In the overdamped case, when the damping is much larger than the frequency of the oscillator, the effective oscillator frequency becomes $\Omega\cong i(\gamma/2)(1-2\omega_0^2/\gamma^2)$ and the response function reduces to

$$r(t)\cong N(m_i\gamma_i)^{-1}[e^{-\omega_i^2 t/\gamma_i}-e^{-\gamma_i t}]\theta(t). \tag{18}$$

In the frequency domain, this corresponds to the type of Lorentzian that is typically used to model the low frequency rotational-diffusion part of the spectrum. In the overdamped response function, the damping rate of the Brownian oscillator γ_i appears as a rate of rise. The overdamped decay rate is a combination of the Brownian-oscillator frequency and decay rate.

III. EXPERIMENT

IR and Raman spectra of liquids have been taken with a variety of techniques. Low frequency IR spectra ($0-100\ \mathrm{cm}^{-1}$) have been taken with sub-picosecond terahertz (THz) pulses. High frequency IR spectra ($50-500\ \mathrm{cm}^{-1}$) have been taken with a Fourier-transform IR spectrometer. Raman spectra have been taken using the optical heterodyne-detected optical Kerr-effect (OHD-RIKES) technique. These experimental techniques will be described briefly here and are reviewed elsewhere.[9,38]

THz pulses have been generated by optical rectification of femtosecond optical pulses. For the THz experiments, the femtosecond pulses came from a commercial laser system producing 800-nm 150-fs FWHM pulses at a repetition rate of 250 kHz and 4 μJ/pulse. This optical beam was split into a strong pump beam (90%) and a relatively weak gate beam. The pump beam was focused by a 5-cm focal-length lens a

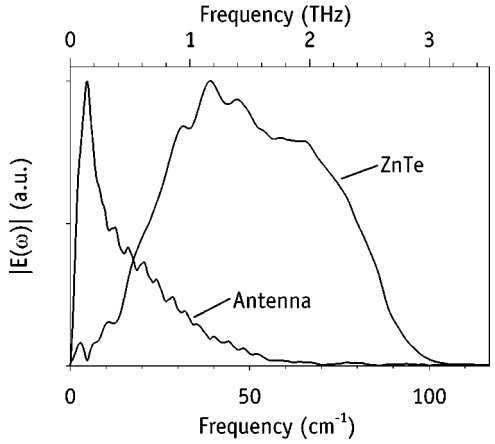

FIG. 2. Spectra of the THz pulses used in the experiments. In both cases, the THz pulses were detected by electro-optic sampling in ⟨110⟩ ZnTe. Generation in a dc biased SIGaAs photoconductive antenna yields useful power up to about 65 cm^{-1}. Rectification in a ZnTe crystal leads to a pulse with the largest bandwidth and an intensity that is about an order of magnitude lower.

few millimeters in front of a crystal to produce a beam of linearly polarized THz radiation. Two different methods have been used to generate the THz radiation. To cover the low-frequency range ($1-50\ cm^{-1}$), an antenna has been used consisting of two strips of silver paint on a semi-insulating GaAs wafer, 5-mm long, and separated by 5 mm, biased by a 1-kV dc potential.[41] To access the high-frequency range ($10-90\ cm^{-1}$), THz radiation has been generated in a 1.15-mm ⟨110⟩-cut ZnTe crystal through optical rectification.[44,45,47] Focusing in the ZnTe crystal results in two-photon absorption and reduction of the THz intensity. Four off-axis parabolic mirrors with a 10-cm focal length and 7.5-cm diameter were used to recollimate, focus onto the sample, recollimate again, and focus onto the detector. The THz beam and the gate beam were recombined on a 5-μm thickness nitrocellulose pellicle beamsplitter, and focused onto an electro-optic sampling (EOS) detector crystal, which is another 1.15-mm ⟨110⟩-cut ZnTe crystal. The induced ellipticity of the optical gate beam in the EOS crystal under the influence of the THz electric field was detected by balanced detection using a quarter-wave plate and a pair of balanced photodiodes.[70] The output of the photodiode pair was sent to a lock-in amplifier. Since the electric field is measured rather than the intensity, this setup allows the measurement of both the absorption and the refractive index of a sample placed in the beam. The gate beam was sent through an optical delay line equipped with a dc motor with a resolution of 0.1 μm. The entire THz beam path was enclosed by a box with a dry-nitrogen atmosphere.

The THz pulse generated in ZnTe has a spectrum (see Fig. 2) peaking at 50 cm^{-1} and has usable power from 1 to 90 cm^{-1}. When taking the spectra in the THz domain, the samples were held between two 8-mm thickness *z*-cut quartz windows. Mylar spacers were used to get samples of the proper thickness. Solvent spectra have been obtained in the high-frequency THz range ($3-80\ cm^{-1}$) by using ZnTe as the generation crystal and using time-domain scans from -5 to 10 ps with a step size of 30 fs. Low-frequency solvent spectra ($0.5-15\ cm^{-1}$) have been obtained by using the biased antenna as a THz-generation source and making time-domain scans from -10 to 100 ps with a 100-fs step size.

A Fourier-transform IR (FTIR) spectrometer has been used to cover the range from 50 cm^{-1} and upward. The spectrometer used was a Bruker IFS 66V equipped with a detector sensitive to the far IR (an Infrared Laboratories LN-6/C bolometer with a filter for the $20-500\ cm^{-1}$ range). The samples were held between two windows separated by Mylar spacers. Two window materials were used, either TPX [poly(4-methyl-1-pentene)] or Teflon. Unfortunately, organic solvents tend to weaken these polymers, which results in some buckling of the windows and therefore some uncertainty in the determination of the thickness of the samples. Hence, the absolute magnitude of the liquid absorption was obtained from the THz data.

Thus, the solvent IR spectra consist of three slices: Low-frequency THz, high-frequency THz, and FTIR data. The high-frequency THz data was considered the most reliable and was therefore used to calculate the absolute absorption of the samples. The FTIR absorption data was scaled in such a way that there was good overlap with the high-frequency THz data in the range $50-75\ cm^{-1}$. The high-frequency THz absorption data above 75 cm^{-1} was subsequently deleted. The refractive-index data is considered valid up to frequencies as high as 100 cm^{-1}. The low-frequency THz data is reliable from about 1 to 50 cm^{-1} and was found to be virtually identical to the high-frequency THz data in the range of overlap. The low-frequency THz data was scaled (by no more than $\pm 10\%$) to the high-frequency THz data where necessary and the data above about 20 cm^{-1} was deleted. To obtain the refractive index at zero frequency, the square root of the static dielectric constant was used.[71–73] The IR absorption and refractive-index spectra thus obtained for benzonitrile, benzyl alcohol, *N*,*N*-dimethylformamide (DMF), ethylene glycol, and glycerol triacetate (GTA) are shown in Fig. 3.

The Raman spectra of the liquids have been obtained using the optical heterodyne-detected optical Kerr-effect technique (OHD-RIKES). Optical femtosecond laser pulses were generated in a homebuilt Ti:sapphire-based oscillator producing 19-fs pulses at 800 nm with a repetition rate of 84-MHz, and ~300-mW average power. A prism compressor has been used to impart a negative chirp onto the laser pulses exactly matching the positive dispersion of the experimental setup. The beam is split in a pump and a probe beam, and focused into the sample with a 6-cm focal length lens. The relative delay between the pump and the probe is adjusted in an optical delay line equipped with a dc motor with an accuracy of 50-nm. The pump and probe beams pass through equivalent amounts of optical material in order to balance the optical dispersion experienced by the two beams. The samples consist of 1-mm path length Homosil-glass cuvettes. After the sample, the probe beam is recollimated, passed through a quarter-wave plate and a Glann–Thomson polarizer, and is detected by a balanced pair of photodiodes. The quarter-wave plate was adjusted such that when there is no signal present, the photodiode pair produces no current. Any ellipticity on the probe beam will result in the balance between the diodes being disturbed and the production of a

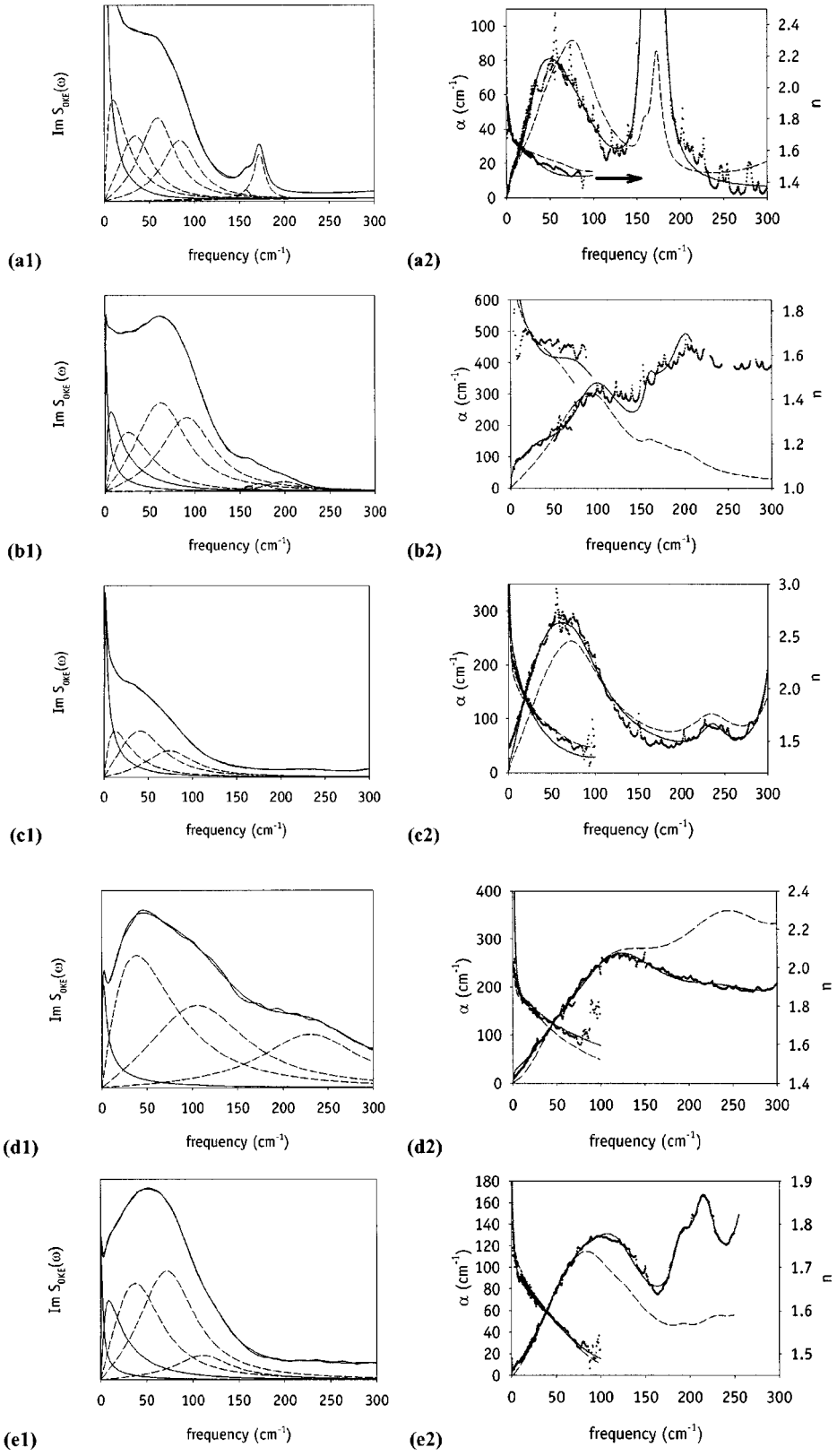

FIG. 3. Optical heterodyne-detected Raman-induced Kerr-effect (OHD-RIKES) data and fits to Brownian oscillators functions (**a1**)–(**e1**) and IR-absorption and refractive-index spectra (**a2**)–(**e2**) of various liquids taken with a combination of Terahertz-spectroscopy techniques and Fourier-transform IR spectroscopy. (**a**) Benzonitrile, (**b**) benzyl alcohol, (**c**) *N*,*N*-dimethylformamide, (**d**) ethylene glycol, and (**e**) glycerol triacetate. Reliable OHD-RIKES data were obtained and fitted to from 0.3 to $\sim 600\ cm^{-1}$. In the OHD-RIKES spectra (**a1**)–(**e1**), the main solid lines represent the experimental data and the fit described in the text and in Table II. The individual contributions to the fit have also been indicated (solid lines for overdamped Lorentzians and dashed lines for Brownian oscillators). In the IR spectra (**a2**)–(**e2**), crosses denote the experimental data, dashed lines denote a straight conversion from the OHD-RIKES spectrum to an IR spectrum, and the solid line denotes a refit of all the amplitudes (see text and Table III).

signal current. Using the Jones-matrix formalism, it can be shown that the signal detected in this fashion is equal to the sine of the (pump-induced) retardation of the sample.[68] The effective laser-pulse duration was determined by autocorrelation at the position of the sample using the two-photon absorption induced photocurrent in a GaP photodiode. The prism compressor positioned before the OHD-RIKES setup was adjusted to obtain the minimum pulse duration (19 fs) at the position of the sample.

The OHD-RIKES spectrum was obtained from the time-domain data using numerical Fourier transformation and deconvolution with the Fourier transform of the autocorrelation

of the laser pulses. It was found that, from experiment to experiment, the zero delay could be controlled with an accuracy no better than a few femtoseconds. Although these slight delay shifts were taken into account in the data analysis, they may lead to systematic errors in the spectra that become progressively worse at higher frequencies. Therefore, our OHD-RIKES setup can take spectra up to a maximum frequency of about 1000 cm^{-1} but they become less reliable above about 500 cm^{-1}.

The solvents used in the experiments were of the highest available purity, purchased from Sigma/Aldrich and used without further purification. Nonlinear least-squares fitting of the data to analytical functions has been performed with a program based on the simplex algorithm.[74] In cases where two data sets had to be fitted simultaneously, i.e., absorption and refractive index, the data were scaled in such a way that both data sets had about equal absolute magnitude. The uncertainties listed for the parameter values of the nonlinear fits, are 1σ joint-confidence intervals,[75] that is, they take into account the cross-correlation between the parameters.

TABLE I. Three ways of fitting the low-frequency part of the OHD-RIKES spectrum of benzyl alcohol. L_1 and L_2 are the amplitudes of overdamped Lorentzian components, γ_{decay} and γ_{rise} are their rate of decay and rise [see Eq. (19)], B_1 to B_4 are the amplitudes of Brownian-oscillator components, and ω_i and γ_i are their frequency and damping rate [see Eq. (16)].

	Fit 1	Fit 2	Fit 3
L_1:	3.4±0.1	3.4±0.15	3.3±0.1
γ_{decay} (cm^{-1}):	1.18±0.03	1.17±0.03	1.16±0.03
γ_{rise} (cm^{-1}):	73	73	72±1.7
L_2:	12±1		12±1
$\gamma_{\text{decay},2}$ (cm^{-1})	7.6±0.5		7.4±0.5
B_1:		800±6800	
ω_1 (cm^{-1}):		24±88	
γ_1 (cm^{-1}):		81±550	
B_2:	2300±1400	2300±9400	1400±53
ω_2 (cm^{-1}):	47±9	47±53	40±1
γ_2 (cm^{-1}):	90±26	90±150	γ_{rise}
B_3:	3300±2200	3300±4600	4300±150
ω_3 (cm^{-1}):	71±5	70±6	71.2±0.9
γ_3 (cm^{-1}):	67±15	67±29	γ_{rise}
B_4:	5400±1600	5400±2200	5100±230
ω_4 (cm^{-1}):	97±2	97±3	97.8±0.7
γ_4 (cm^{-1}):	73±4	73±5	γ_{rise}

IV. RESULTS AND DISCUSSION

Figures 3(a1)–3(e1) show the experimental OHD-RIKES spectra in benzonitrile, benzyl alcohol, *N*,*N*-dimethylformamide, ethylene glycol, and glycerol triacetate with fits to a sum of Brownian-oscillator response functions. In the time-domain OHD-RIKES experiments, data were collected at low time-resolution (50 fs) out to long time delays ($\approx$100 ps). As there is always a very small ($\sim$0.1% of peak signal) background due to scattered pump light, a linear curve was first subtracted from the data. Next the data in the time domain were tail fitted, that is, an exponential decay was fitted to the data at delays $>$5 ps. This slow exponential decay is due rotational diffusion, which takes place on a time scale ranging from a few picoseconds to $\sim$100 ps. However, due to the very small signal at long delays in combination with the small background of scattered pump light, it is very difficult to extract an accurate rotational-diffusion decay time from these data. Therefore, it was decided neither to use this decay time as a fixed parameter in the fits to the spectra, nor to subtract the exponential tail from the data.

The low-frequency part of the spectrum corresponding with rotational diffusion in the liquid, was fitted with the Fourier transform of

$$r_i(t) = L_i \theta(t)[e^{-\gamma_{i,\text{decay}} t} - e^{-\gamma_{i,\text{rise}} t}], \tag{19}$$

which is equivalent to Eq. (18) if one sets $\gamma_{i,\text{decay}} \equiv \omega_i^2/\gamma_i$ and $\gamma_{i,\text{rise}} \equiv \gamma_i$. The rise time $\gamma_{i,\text{rise}}^{-1}$ was initially set equal to the first moment of the low frequency part of the spectrum[76] arbitrarily judged to be from 0 to about 200 cm^{-1}. The precise value of this rise time has only a minor effect on the values of the other parameters. The spectra were initially fitted with one overdamped-oscillator function [the Fourier transform of Eq. (19)] and one or two underdamped oscillator functions [Eq. (17)] with all the parameters (amplitudes, frequencies, and damping rates) left free to change except for the rise time $\gamma_{i,\text{rise}}^{-1}$ of the overdamped component. If required additional oscillators were added one by one, until a satisfactory fit was obtained.

Table I shows three ways the OHD-RIKES data from benzyl alcohol could be fitted. Fit 1 fits the data to two overdamped Lorentzian components and three Brownian oscillators. The rate of rise for both Lorentzians has been fixed to the first moment of the spectrum (73 cm^{-1}) but they have independent decay rates. In fit 2, one overdamped Lorentzian has been replaced by a Brownian oscillator, with little to no effect on the parameters. One of the interesting things that can be seen in fits 1 and 2 is that the decay rates of the Brownian oscillators (81, 90, 67, and 73 cm^{-1} in fit 2) are all indistinguishable from the first moment of the spectrum (73 cm^{-1}) within the signal to noise ratio. This is not wholly surprising within the Brownian-oscillator model: Each of the ''important'' modes is damped by coupling to the bath of all possible motions in the liquid. Hence, each oscillator is on average coupled to the same bath resulting in fluctuations with a given correlation time. There is no *a priori* physical reason why the coupling strength to the bath would be the same for all oscillators. However, the motions studied here (in the frequency range $\sim$10–150 cm^{-1}) all have librational character and could therefore be coupled to the bath with similar enough strengths as to be experimentally indistinguishable. Fit 3 shows a fit where the rise rate of the Lorentzians and the decay rate of the Brownian oscillators have all been coupled. This final procedure was used to analyze all the OHD-RIKES data. (See Table II.)

Figures 3(a2)–3(e2) shows the experimental IR-absorption and refractive-index spectra of the same set of five liquids. As described in the Theory, in some simple cases it may be possible to calculate the IR spectrum of the solvent with some accuracy simply from the fit to the OHD-RIKES spectrum and by multiplying it with a simple scaling function. The dashed line in Figs. 3(a2)–3(e2) is the IR spectrum

TABLE II. Parameters obtained from fits to the OHD-RIKES data. The meaning of the parameters is the same as in Table I. As in fit 3 in Table I, the decay rates of the Brownian-oscillator components have been set equal to the rise rate of the Lorentzian component, i.e., $\gamma_1=\gamma_2=\gamma_3=\gamma_{\text{rise}}$. The amplitudes of the components of the fit (L_1, L_2, B_1, B_2, and B_3) are in arbitrary units and cannot be compared between liquids.

	Benzonitrile	Benzyl alcohol	DMF	Ethylene glycol	GTA
L_1:	19.0±0.2	3.3±0.1	5.93±0.08	0.13±0.01	0.32±0.01
γ_{decay} (cm^{-1}):	0.577±0.007	1.16±0.03	1.59±0.02	2.1±0.2	0.77±0.03
γ_{rise} (cm^{-1}):	49±3	72±2.2	70±1.5	135±8	76±3
L_2	51±7	12±1			2.5±0.2
$\gamma_{\text{decay},2}$ (cm^{-1})	11.2±0.9	7.4±0.5			9.3±0.5
Calculated first moment (cm^{-1})	54	73	45	129	62
B_1:	2440±280	1400±55	680±30	280±20	530±28
ω_1 (cm^{-1}):	42±2	40±1	28.3±0.5	67±2	51±1
γ_1 (cm^{-1}):	γ_{rise}	γ_{rise}	γ_{rise}	γ_{rise}	γ_{rise}
B_2:	5000±350	4300±150	1640±44	390±20	1030±49
ω_2 (cm^{-1}):	64±2	71.2±0.9	52.1±0.8	124±3	81±1
γ_2 (cm^{-1}):	γ_{rise}	γ_{rise}	γ_{rise}	γ_{rise}	γ_{rise}
B_3:	5100±490	5100±250	1570±58	510±58	340±34
ω_3 (cm^{-1}):	88±2	97.8±0.8	81.8±0.9	240±4	117±3
γ_3 (cm^{-1}):	γ_{rise}	γ_{rise}	γ_{rise}	γ_{rise}	γ_{rise}

calculated in this fashion (and scaled by a factor to obtain similar amplitudes). It can be seen that the shape of the low-frequency IR spectrum thus calculated is surprisingly similar to the actual IR spectrum but certainly not identical. Initially, the experimental IR spectra were fitted by fixing the fit parameters found by fitting the OHD-RIKES spectra and optimizing the overall amplitude and the refractive index at infinite frequency (n_∞). In the next step, the amplitudes of the individual components of the fit functions (L_i and B_i) were allowed to vary. This resulted in a very much improved fit shown as the solid line in Figs. 3(a2)–3(e2). The parameters of these fits and their statistical uncertainties are listed in Table III.

The rotational-diffusion component of the OHD-RIKES and IR spectra requires further discussion. In the time domain, the long-time decay in OHD-RIKES and the IR free induction decay are proportional to the temporal derivative of the orientational correlation function of appropriate order. This correlation function is typically expressed as

$$r_l(t)=\langle P_l[\boldsymbol{\mu}(t)\cdot\boldsymbol{\mu}(0)]\rangle=\exp[-l(l+1)Dt], \qquad (20)$$

where P_l is the Legendre polynomial of order l and D is the Debye rotational-diffusion rate. The order is $l=1$ for IR and $l=2$ for Raman/OHD-RIKES and thus it would be expected that the rotational decay rate (γ_{decay}) required to fit the IR data is three times smaller than that required to fit the OHD-RIKES data. Testing this experimentally would require a good signal-to-noise ratio in the IR spectra in the range $0.01-1\ \text{cm}^{-1}$, which is not available. In practice, the fit to the IR spectra does not change appreciably when γ_{decay} is divided by three. In the fits in Figs. 3(a2)–3(e2), γ_{decay} has been divided by 3 for consistency.

V. CONCLUSION

Here we have studied five different polar liquids with OHD-RIKES and analyzed the spectra with the Brownian-oscillator model. It had previously been reported that fitting with Lorentzian, Ohmic, and Gaussian functions gave better fit results, especially at higher ($>100\ \text{cm}^{-1}$) frequencies. The explanation had been that the low-frequency intermolecular Raman spectrum was inhomogeneously broadened,[34,77] for example, because of an inhomogeneous distribution of cages that librating molecules find themselves in or because of collisional broadening effects.[32] Here it is found that fitting to a small set of homogeneously broadened Brownian oscillators gives rise to a satisfactory fit as well. It is difficult to quantify the quality of the various ways of fitting because the random noise in the data may be smaller than potential systematic errors. In principle, a small error in the determination of zero delay can raise (or lower) the spectrum at high frequencies giving the appearance of the spectral ''tail'' normally associated with the wing of a Lorentzian (homogeneously broadened) line. However, we have gone at great lengths to avoid these systematic errors. The OHD-RIKES spectra presented here have been analyzed (''baseline corrected'') up to $800-1000\ \text{cm}^{-1}$. Therefore, any systematic errors should be negligible in the range $0-500\ \text{cm}^{-1}$.

Fitting the low-frequency intermolecular spectra of the five polar liquids requires four or five oscillators: One or two overdamped (Lorentzian) functions and three Brownian oscillators. Typically, a number of additional Brownian oscillators have been used to fit higher frequency intramolecular Raman lines. The fits could have been marginally improved by including an inhomogeneous distribution of the frequency of each oscillator[77] but this would have greatly complicated and confused the analysis. Of course, the use of a number of oscillators (four or five instead of one) in fitting the data implies a degree of inhomogeneity in the liquid. However, given the structurelessness of OHD-RIKES spectra of liquids and the high quality of the fits that have been obtained here, it can be concluded that there is no compelling reason to assume that the low-frequency intermolecular nuclear motions in the five liquids studied here are not simply homogeneously broadened. This conclusion is consistent with, for example, Raman-echo studies of higher frequency intramolecular vibrational modes in liquids.[35] In principle, higher

TABLE III. Comparison of amplitudes between OKE and IR. The original amplitudes for the OKE data are the same as in Table II and the amplitudes for the IR data are obtained by refitting. As the absolute values of the amplitudes cannot be compared between liquids, the amplitudes have been rescaled by setting those of the first Brownian oscillator equal to one. All the other parameters have been kept the same except γ_{decay} and $\gamma_{decay,2}$ if appropriate have been divided by three for the fits to the IR spectra.

	Benzonitrile		Benzyl alcohol		DMF		Ethylene glycol		GTA	
	OKE	IR	OKE	IR	OKE	IR	OKE	IR	OKE	IR
$L1\times100$:	0.78±	0±	0.236±	2.5±	0.87±	0.52±	0.046±	0.36±	0.06±	0.131±
	0.01	0.1	0.007	1.4	0.01	0.09	0.004	0.04	0.002	0.005
$L2\times100$:	2.1±	0.7±	0.86±	0					0.47±	0.24±
	0.3	0.2	0.07						0.04	0.04
B_1:	1.0±	1.0±	1.00±	1.0±	1.00±	1.0±	1.00±	1.0±	1.00±	1.00±
	0.1	0.08	0.04	1.3	0.04	0.1	0.07	0.09	0.05	0.06
B_2:	2.0±	0.46±	3.1±	0±	2.41±	1.0±	1.39±	2.1±	1.9±	1.29±
	0.1	0.09	0.1	1.2	0.06	0.1	0.07	0.1	0.1	0.07
B_3:	2.1±	0.24±	3.6±	4.4±	2.31±	0.67±	1.8±	0.7±	0.64±	1.60±
	0.2	0.07	0.2	0.9	0.09	0.09	0.2	0.2	0.06	0.06
n_∞:	···	1.46±	···	1.4±	···	1.47±	···	1±	···	1.46±
		0.01		0.2		0.40		10		0.1

order OHD-RIKES-like experiments[21–24] could distinguish between homogeneous and inhomogeneous broadening of the low-frequency intermolecular modes but in practice this has not been possible yet.[20,25] We have recently shown[68] that the analysis of OHD-RIKES spectra in terms of a small set of Brownian oscillators provides the simplification needed to understand liquid dynamics better. The OHD-RIKES spectra of a set of room-temperature organic ionic liquids could be understood in terms of the local structure of the liquid around the cation with three Brownian oscillators corresponding to libration of the cation at three slightly different frequencies corresponding to three positions of the anion with respect to the cation.

It has been found that when the OHD-RIKES spectra are fitted to a small number of oscillators, the decay rates (or rather, the decay rates for Brownian oscillators and the equivalent rise rates for Lorentzians) tend to a single value for a given liquid (see Table I). This is consistent with a picture in which the ultrafast liquid dynamics is described by a small number of ''important'' modes, which are homogeneously damped by the weak and rapid fluctuations of other bath modes.

Here we have also presented the IR spectra of the same five polar organic liquids. Collecting high-quality IR spectra in the range 0 to $>300\,cm^{-1}$ is much more difficult than collecting Raman (OHD-RIKES) spectra. The spectra presented here have been patched together from spectra taken with THz pulses produced in photoconductive antennas, with THz pulses produced by optical rectification, and IR spectra taken with an FTIR equipped with a bolometric detector. Collecting far-IR spectra is made very difficult by the strong absorption of the liquids themselves (requiring thin 25 μm–0.5 mm samples), Fabry–Perot effects, absorption by the windows of the sample cells used, absorption by optics (e.g., beamsplitters in a FTIR), absorption by water vapor, noise in the detectors (i.e., bolometers), and absorption by THz generators and detectors. The IR absorption and refractive-index spectra presented in Figs. 3(a2)–3(e2) certainly cannot be used for the sort of detailed analysis that is possible with OHD-RIKES spectra. Further development of THz technology might make such an analysis possible in the future.

The conversion from OHD-RIKES spectra to IR spectra shown in Fig. 3 is reasonably successful. Simply scaling the OHD-RIKES spectra according to the general formulas does not describe the IR spectra very well. This is expected as the amplitude of the low-frequency intermolecular IR spectra depends mostly on the permanent dipole moment whereas that of the OHD-RIKES spectra mostly depends on the anisotropy of the intrinsic (electronic) polarizability. In addition, the amplitudes in the IR spectra are influenced by collision-induced dipoles[52,60,64] and those in the OHD-RIKES spectra by collision-induced polarizabilities.[32,78] However, refitting the amplitudes of the individual oscillators (while keeping frequency and damping the same) does lead to a good correspondence within the signal to noise ratio between the converted Raman spectrum and the experimental IR spectrum. Only at higher frequencies (above about $200\,cm^{-1}$) where intramolecular modes exhibit IR absorption are the deviations significant. Table III compares the scaled amplitudes of the Brownian-oscillator and Lorentzian components. The correspondence is reasonable (within about a factor of 2) for the (relatively high frequency) Brownian oscillators and very poor for the (low frequency) Lorentzian components. As collision-induced, collective, and translational motions are expected to be of greater importance at low frequencies[11,33,60,66] it is perhaps not surprising that the correspondence breaks down at the low-frequency end of the spectrum. Unfortunately, the signal-to-noise ratio of the IR spectra is not good enough to make this a definitive test. However, we tentatively conclude that the description in terms of a small number of harmonic modes that are both Raman and IR active is valid at intermediate frequencies (~20 to $\sim200\,cm^{-1}$) where the dynamics can be understood in terms of the libration of individual molecules coupled to a bath damping these modes. In another study,[11] it had been concluded that there is no simple relationship between OHD-RIKES and dielectric measurements at long time scales or low frequencies. This conclusion is consistent with the present work, which only finds a relationship at

intermediate frequencies and not at the low-frequency end of the spectrum.

This conclusion is relevant, for example, in the theoretical description of chemical reactions in solution involving rearrangements of the charge distribution such as proton or electron transfer. Higher precision in rate calculations could be obtained by replacing a single solvent coordinate[79,80] by four or five depending on the solvent. In addition, some of these solvent coordinates are overdamped and some are underdamped. Low-frequency modes have now also been observed in the OHD-RIKES spectra of peptides and proteins.[14–16] It may be expected that these protein modes will play a similar role in biomolecular reactions as intermolecular modes in liquids do. However, as the anisotropy in the polarizability tensor associated with these protein modes is not known, the OHD-RIKES spectra of proteins cannot be used directly to calculate solvation dynamics in proteins.

ACKNOWLEDGMENTS

We gratefully acknowledge experimental support from Jan Karolin, Ilya Fedorov, Anne-Katrin Klehe, and John Singleton. The experiments were performed in the Femtosecond Research Center (FRC) at Strathclyde University. Acknowledgement is also made to the donors of The Petroleum Research Fund, administered by the ACS for support of this research and from EPSRC.

[1] P. F. Barbara, T. J. Meyer, and M. A. Ratner, J. Phys. Chem. **100**, 13148 (1996).
[2] K. Wynne and R. M. Hochstrasser, Adv. Chem. Phys. **107**, 263 (1999).
[3] G. A. Voth and R. M. Hochstrasser, J. Phys. Chem. **100**, 13034 (1996).
[4] M. D. Newton and N. Sutin, Annu. Rev. Phys. Chem. **35**, 437 (1984).
[5] H. Sumi and R. A. Marcus, J. Chem. Phys. **84**, 4894 (1986).
[6] J. Jortner and M. Bixon, J. Chem. Phys. **88**, 167 (1988).
[7] R. F. Grote and J. T. Hynes, J. Chem. Phys. **73**, 2715 (1980).
[8] S. Park, B. N. Flanders, X. Shang, R. A. Westervelt, J. Kim, and N. F. Scherer, J. Chem. Phys. **118**, 3917 (2003).
[9] N. A. Smith and S. R. Meech, Int. Rev. Phys. Chem. **21**, 75 (2002).
[10] B. I. Greene and R. C. Farrow, Chem. Phys. Lett. **98**, 273 (1983).
[11] E. W. Castner and M. Maroncelli, J. Mol. Liq. **77**, 1 (1998).
[12] K. Winkler, J. Lindner, and P. Vohringer, Phys. Chem. Chem. Phys. **4**, 2144 (2002).
[13] A. Idrissi, P. Bartolini, M. Ricci, and R. Righini, J. Chem. Phys. **114**, 6774 (2001).
[14] G. Giraud and K. Wynne, J. Am. Chem. Soc. **124**, 12110 (2002).
[15] G. Giraud, J. Karolin, and K. Wynne, Biophys. J. **85**, 1903 (2003).
[16] J. D. Eaves, C. J. Fecko, A. L. Stevens, P. Peng, and A. Tokmakoff, Chem. Phys. Lett. **376**, 20 (2003).
[17] B. J. Loughnane, R. A. Farrer, A. Scodinu, T. Reilly, and J. T. Fourkas, J. Phys. Chem. B **104**, 5421 (2000).
[18] O. Golonzka, N. Demirdoven, M. Khalil, and A. Tokmakoff, J. Chem. Phys. **113**, 9893 (2000).
[19] L. J. Kaufman, D. A. Blank, and G. R. Fleming, J. Chem. Phys. **114**, 2312 (2001).
[20] K. J. Kubarych, C. J. Milne, S. Lin, V. Astinov, and R. J. D. Miller, J. Chem. Phys. **116**, 2016 (2002).
[21] Y. Tanimura and S. Mukamel, J. Chem. Phys. **99**, 9496 (1993).
[22] V. Khidekel and S. Mukamel, Chem. Phys. Lett. **240**, 304 (1995).
[23] T. Steffen, J. T. Fourkas, and K. Duppen, J. Chem. Phys. **105**, 7364 (1996).
[24] V. Chernyak and S. Mukamel, J. Chem. Phys. **108**, 5812 (1998).
[25] J. C. Kirkwood and A. C. Albrecht, J. Raman Spectrosc. **31**, 107 (2000).
[26] P. F. Barbara and W. Jarzeba, Adv. Photochem. **15**, 1 (1990).
[27] W. P. de Boeij, M. S. Pshenichnikov, and D. A. Wiersma, Chem. Phys. **233**, 287 (1998).
[28] M. Cho, S. J. Rosenthal, N. F. Scherer, L. D. Ziegler, and G. R. Fleming, J. Chem. Phys. **96**, 5033 (1992).
[29] M. Cho, M. Du, N. F. Scherer, G. R. Fleming, and S. Mukamel, J. Chem. Phys. **99**, 2410 (1993).
[30] T.-S. Yang, P. Vöhringer, D. C. Arnett, and N. F. Scherer, J. Chem. Phys. **103**, 8346 (1995).
[31] T. S. Perova, J. K. Vij, D. H. Christensen, and O. F. Nielsen, J. Mol. Struct. **479**, 111 (1999).
[32] J. A. Bucaro and T. A. Litovitz, J. Chem. Phys. **54**, 3846 (1971).
[33] B. M. Ladanyi and S. Klein, J. Chem. Phys. **105**, 1552 (1996).
[34] B. Ratajska-Gadomska, J. Chem. Phys. **116**, 4563 (2002).
[35] D. Vandenbout, L. J. Muller, and M. Berg, Phys. Rev. Lett. **67**, 3700 (1991).
[36] R. M. Stratt, Acc. Chem. Res. **28**, 201 (1995).
[37] A. Ma and R. M. Stratt, J. Chem. Phys. **116**, 4972 (2002).
[38] M. C. Beard, G. M. Turner, and C. A. Schmuttenmaer, J. Phys. Chem. B **106**, 7146 (2002).
[39] Y. Cai, I. Brener, J. Lopata, J. Wynn, L. Pfeiffer, and J. Federici, Appl. Phys. Lett. **71**, 2076 (1997).
[40] R. McElroy and K. Wynne, Phys. Rev. Lett. **79**, 3078 (1997).
[41] J. J. Carey, J. Zawadzka, D. A. Jaroszynski, and K. Wynne, Phys. Rev. Lett. **84**, 1431 (2000).
[42] K. Wynne, J. J. Carey, J. Zawadzka, and D. A. Jaroszynski, Opt. Commun. **176**, 429 (2000).
[43] Q. Wu and X.-C. Zhang, Appl. Phys. Lett. **70**, 1784 (1997).
[44] J. J. Carcy, R. T. Bailcy, D. Pugh, J. N. Sherwood, F. R. Cruickshank, and K. Wynne, Appl. Phys. Lett. **81**, 4335 (2002).
[45] Q. Wu and X. C. Zhang, Appl. Phys. Lett. **71**, 1285 (1997).
[46] P. Y. Han and X.-C. Zhang, Appl. Phys. Lett. **73**, 3049 (1998).
[47] A. Nahata, A. S. Weling, and T. F. Heinz, Appl. Phys. Lett. **69**, 2321 (1996).
[48] J. E. Pedersen and S. R. Keiding, IEEE J. Quantum Electron. **28**, 2518 (1992).
[49] B. N. Flanders, R. A. Cheville, D. Grischkowsky, and N. F. Scherer, J. Phys. Chem. **100**, 11824 (1996).
[50] S. R. Keiding, J. Phys. Chem. A **101**, 5250 (1997).
[51] C. Rønne, K. Jensby, B. J. Loughnane, J. Fourkas, O. F. Nielsen, and S. R. Keiding, J. Chem. Phys. **113**, 3749 (2000).
[52] T. M. Nymand, C. Rønne, and S. Keiding, J. Chem. Phys. **114**, 5246 (2001).
[53] J. T. Kindt and C. A. Schmuttenmaer, J. Phys. Chem. **100**, 10373 (1996).
[54] C. Rønne, L. Thrane, P. O. Åstrand, A. Wallqvist, K. V. Mikkelsen, and S. Keiding, J. Chem. Phys. **107**, 5319 (1997).
[55] D. S. Venables and C. A. Schmuttenmaer, J. Chem. Phys. **108**, 4935 (1998).
[56] B. N. Flanders, X. Shang, N. F. Scherer, and D. Grischkowsky, J. Phys. Chem. A **103**, 10054 (1999).
[57] D. S. Venables and C. A. Schmuttenmaer, J. Chem. Phys. **113**, 11222 (2000).
[58] M. L. T. Asaki, A. Redondo, T. A. Zawodzinski, and A. J. Taylor, J. Chem. Phys. **116**, 10377 (2002).
[59] B. J. Bernc and G. D. Harp, Adv. Chem. Phys. **17**, 63 (1970).
[60] J. T. Kindt and C. A. Schmuttenmaer, J. Chem. Phys. **106**, 4389 (1997).
[61] Y. R. Shen, *The Principles of Nonlinear Optics* (Wiley, New York, 1986).
[62] Y. J. Yan and S. Mukamel, J. Chem. Phys. **94**, 997 (1991).
[63] S. Mukamel, *Principles of Nonlinear Optical Spectroscopy* (Oxford University Press, New York, 1995).
[64] G. P. Johari, J. Non-Cryst. Solids **307-310**, 114 (2002).
[65] X. Ji, H. Alhborn, B. Space, P. B. Moore, Y. Zhou, S. Constantine, and L. D. Ziegler, J. Chem. Phys. **112**, 4186 (2000).
[66] M. Paolantoni and B. M. Ladanyi, J. Chem. Phys. **117**, 3856 (2002).
[67] N. G. v. Kampen, *Stochastic Processes in Physics and Chemistry* (North-Holland, Amsterdam, 1992).
[68] G. Giraud, C. Gordon, I. R. Dunkin, and K. Wynne, J. Chem. Phys. **199**, 464 (2003).
[69] Y.-J. Yan and S. Mukamel, J. Chem. Phys. **89**, 5160 (1988).
[70] G. D. Reid and K. Wynne, in *Encyclopedia of Analytical Chemistry: Instrumentation and Applications* (Wiley, New York, 2000).
[71] J. A. Riddick, W. B. Bunger, and T. K. Sakano, *Organic Solvents: Physical Properties and Methods of Purification*, 4th ed. (Wiley, New York, 1986).
[72] *Handbook of Chemistry and Physics*, 57th ed. (CRC, Boca Raton, 1977).

[73] E. Ikada and T. Watanabe, J. Phys. Chem. **78**, 1078 (1974).
[74] W. H. Press, S. A. Teukolsky, W. T. Vetterling, and B. P. Flannery, *Numerical Recipes in C*, 2nd ed. (Cambridge University Press, New York, 1995).
[75] G. A. Seber and C. J. Wild, *Nonlinear Regression* (Wiley, New York, 1989).
[76] Y. J. Chang and E. W. Castner, J. Chem. Phys. **99**, 7289 (1993).
[77] D. McMorrow, N. Thantu, V. Kleiman, J. S. Melinger, and W. T. Lotshaw, J. Phys. Chem. A **105**, 7960 (2001).
[78] C. J. Fecko, J. D. Eaves, and A. Tokmakoff, J. Chem. Phys. **117**, 1139 (2002).
[79] E. Åkesson, A. E. Johnson, N. E. Levinger, G. C. Walker, T. P. DuBruil, and P. F. Barbara, J. Chem. Phys. **96**, 7859 (1992).
[80] K. Wynne, C. Galli, and R. M. Hochstrasser, J. Chem. Phys. **100**, 4797 (1994).